ACS OMEGA

http://pubs.acs.org/journal/acsodf

Article

Fabrication of Carbon−Alumina Composites via Catalytic Pyrolysis of Pine Sawdust on Aluminum Dross for Cr(VI) Removal

Peng Liu, Li Liu, Yanling Li, Zhengzhong Zhou,* Taoli Huhe, and Tingzhou Lei*

Cite This: *ACS Omega* 2021, 6, 22301−22310

Read Online

ABSTRACT: Carbon−alumina composites are prepared for the efficient removal of Cr(VI) from wastewater. Pristine and acid-treated alumina dross (AD and AAD) are copyrolyzed with pine sawdust to form the respective composites, ADPC and AADPC. Excellent absorption properties with Cr(VI) removal efficiency of 95.08% are demonstrated at 60 °C for an initial concentration of 6 μg/mL. The composites combine the merits of char, which provides a high surface-to-volume ratio with abundant functional groups on the surface, and alumina, which provides metal ions for coprecipitation. Carbon structures of pine, char, and composite were analyzed semiquantitatively using ^{13}C NMR by a curve-fitting method. Cr(VI) adsorption is accurately described with chemisorption by the Langmuir isotherm model and a pseudo-second-order kinetic model. The results show that AADPC has more alcohol hydroxyl groups substituted to glucosyl units in amorphous cellulose assigned to the peak at 80 ppm and hemicellulose assigned to peaks at 97 and 101 ppm. Also, it has more phenolic groups in lignin distributed at syringyl units assigned to peaks at 129 and 146 ppm. These oxygen-containing functional groups have a significant influence on Cr(VI) adsorption and reduction to Cr(III) governed by the mechanisms of diffusion, adsorption, complexation, reduction, and coprecipitation. The results of this work provide a new direction for the reuse of biomass and industrial solid wastes to fabricate higher value-added products, i.e., adsorption materials for Cr(VI) removal and stabilization.

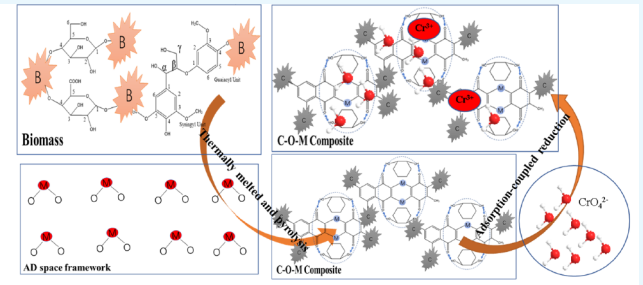

AD- Aluminum dross; B- Biomass; M- Metal; O- Oxygen; C- Char; C-O-M- Carbon-oxygen-metal

1. INTRODUCTION

Water pollution by heavy metals is a major concern for public health. The common processes for removal of heavy metals are hydroxide precipitation, coagulation−flocculation, absorption,[1−3] ion exchange, and membrane separation.[4] Activated alumina is a state-of-the-art sorbent for its low cost, porous structure, and activated hydroxyl sites.[5,6] One of the wastes generated from the aluminum production industry, alumina dross (AD),[7] is also used directly as a sorbent for water purification by other researchers.[8] However, the exchangeable form of heavy metals in the AD may bring about land and water contamination.[9,10] It is necessary to convert the exchangeable form of heavy metals into an immobilized residual form for harmless treatment of AD before application in water purification.

Some research studies discussed the disposal of heavy metals in sorbents using chemical solidification,[11] melting stabilization by thermal plasma,[12] heavy-metal extraction,[13] etc. These methods have some shortcomings, for instance, chemical solidification and heavy-metal extraction cost too much. The technique of melting stabilization by thermal plasma needs to be carried out at high temperatures. A number of research studies on carbonation of sewage sludge[14−17] demonstrated that sewage sludge char produced from the codisposal of sewage sludge and municipal solid waste incineration fly ash can restrain the leaching of heavy metals. Moreover, Leng et al.[18] showed the coliquefaction of municipal sewage sludge and lignocellulosic biomass, which could enhance the immobilization of heavy metal in biochars. Huber et al.[19] also promoted thermal cotreatment of combustible hazardous waste and waste incineration fly ash in a rotary kiln to convert hazardous waste into nonhazardous wastes. The above suggests that the codisposal of organic and hazardous waste through carbonation is a feasible and effective alternative for heavy metal immobilization.

Additionally, char produced from biomass pyrolysis has been used in wastewater treatment as a low-cost sorbent replacing activated carbon. It removes various contaminants from water such as nutrients, trace metals, pharmaceuticals, pesticides, dyes, metal(loids), volatile organic compounds, and polycyclic aromatic hydrocarbons[20−25] because of its multifunctional characteristics, including high stability, high extent of oxygen-

Received: June 8, 2021
Accepted: August 10, 2021
Published: August 18, 2021

containing functional groups (OcFGs), high surface area, and high microporosity.[26] Many researchers studied the biochar from sludge as sorbents[27−30] because it contains considerable organic functional groups and inorganic active mineral oxides, both making significant contributions to metal sorption behavior. Premarathna et al.[31] reviewed biochar-based engineering composites for sorptive decontamination of water, showing that biochar composites prepared by the combination of biochar with different additives, including metals, metal oxides, clay minerals, and carbonaceous materials, exhibit better physicochemical properties and broadened adsorption potential for a wide range of aquatic contaminants. Zhang et al.[32] suggested that biochar can be modified to produce biochar/iron oxide composites with good methylene blue removal capacity. Compared with the biochar, the composite modified using Fe,[33,34] Ca,[34] Mg,[35] Mn[36] or other natural solids[37−40] demonstrates higher affinity to contaminants. Karmacharya et al.[41] showed efficient adsorption and rapid removal of As(III) and As(V) using rubber-tire-derived activated carbon modified with the alumina composite. Moreover, the synergistic effect of alumina and biochar can significantly affect the immobilization pathways of metals in contaminated soils.[42]

Cr(VI) is of particularly environmental concern due to its toxicity and mobility and is challenging to be removed from industrial wastewater.[27] The "adsorption-coupled reduction" mechanism that reduces Cr(VI) to Cr(III) with carbon materials under acidic conditions is widely accepted.[43−47] The viewpoint inferred here is that carbonation of AD and biomass may not only make the AD harmless but also prepare a very effective environmental sorbent synergizing the merits of alumina and carbon. The "adsorption-coupled reduction" reaction for Cr(VI) removal can be enhanced. The interaction between biomass and AD during pyrolysis is also hardly ever elaborated for preparing the carbon−alumina composite.

The carbon−alumina composite is prepared from AD and pine sawdust through pyrolysis to make AADPC in this study. AD is pretreated by organic acid to optimize the surface structure. The adsorption characteristics of Cr(VI) on the carbon−alumina composite are studied in batch systems with varying parameters of solution pH, initial Cr(VI) concentration, and temperature. The mechanism of Cr(VI) removal using the new carbon−alumina composite was also inferred from the adsorption characteristics. These results demonstrate the method of waste control by waste, which achieved the dual benefits on the environment and economy and will put forward a new direction for disposal and utilization of industrial hazardous wastes.

2. RESULTS AND DISCUSSION

2.1. Effect of AD on Char Carbon Structure from the Process of Preparing the Composite. The main organic carbon structural parameters of char with and without alumina analyzed by ^{13}C NMR are listed in Table 1 (fitted ^{13}C NMR spectra and all of the carbon structures assigned to the chemical shift of biochar are shown in Figure S1 and Table S1).

With the temperature increasing toward 700 °C, the decrease in signals at 68−110 ppm, as shown in Table S1, is the result of carbonate pyrolysis in cellulose and hemicellulose. The representative carbon structures (carbon in cellulose and hemicellulose marked as C1−C6 and the guaiacyl unit (G1−G6) and syringyl unit (S1−S6) marked in lignin) of biomass components are shown in Figure S2. The side chains of aromatic rings in lignin are broken to a certain extent as illustrated by an increase of signal at 116 ppm, which corresponds to proton aromatic carbon. OcFGs, such as ester, carbonyl, and hydroxyl in char, are the main components for the cross-linking reaction to form char so that the signal at 178 ppm increases with increasing temperature. When the AD is added, the area percentage of signals in char at 97, 72, and 15 ppm increases markedly. These C−O bonds in char increase during catalytic pyrolysis, i.e., the area percentage of the signal at 97 ppm, assigned to C4 in hemicelluloses, increases from 3.04% (in PC) to 5.50% (in ADPC), that of the signal at 72 ppm assigned to Cα-substituted aromatic carbon in lignin increases from 0% to 14.38%, and that of the signal at 15 ppm assigned to CH_3−COO− in hemicelluloses increases from 0% to 10.91%. However, the area percentage of the signal assigned to the side chains on aromatics, such as signals at 129 and 146 ppm, increases from 10.51% of pine char to 20.78% of the composite. Meanwhile, the aromatic carbon assigned to 116 ppm in char decreases. These data indicate that AD addition selectively sustains C−O bonds, mostly in hemicellulose in pine.

The pretreatment of AD by organic acid has little impact on the mineral composition of AD, as shown in Table 1. However, the Brunauer−Emmett−Teller (BET) surface area increases from 9.41 to 25.65 m^2/g, as shown in Table 2. The pore size and volume also increase obviously. The change in surface structure results in different carbon structures of AADPC from those of ADPC, as shown in Table 1. As a result of the surface area and pore size increment on AD, more active sites on AD

Table 1. Main Carbon Structural Parameters Assigned to Chemical Shift with Area Percentage of the Biochar and Composite

chemical shift (ppm)	assignments	pine	PC[a]	ADPC[b]	AADPC
178	carbohydrates: −COO−R and CH_3−COO−	0.49	20.26	16.14	
146	lignins: G[e]1(e), G4(e[d]), S[c]3(ne[f]), and S5(ne)	5.84	10.51		15.07
129	lignins: G1(e), S1(ne), and S4(ne)	7.40		20.78	9.28
116	lignins: G6, G2, S6, and S2	3.79	41.91	16.98	26.06
97	hemicelluloses: C4	1.55	3.04	5.50	6.47
80	amorphous celluloses: C4; lignin: Cβ	6.84		1.90	12.71
72	hemicelluloses and cellulose: C2, C3, and C5; lignins: Cα	17.20		14.38	
15	hemicelluloses: CH_3−COO−	3.44		10.91	7.16

[a]PC is from pine pyrolysis at 700 °C. [b]ADPC is char from pyrolysis of pine and aluminum with a mass ratio of 1:1 at 700 °C. [c]S is syringyl unit. [d]e is etherified. [e]G is guaiacyl units. [f]ne is nonetherified.

Table 2. Some Physical Properties of Raw and Treated AD

samples	BET surface area (m^2/g)	average pore size (nm)	pore volume (cm^3/g)
AD	9.41	15.06	0.037
AAD	25.65	18.97	0.116

https://doi.org/10.1021/acsomega.1c02998
ACS Omega 2021, 6, 22301−22310

are produced for char formation on its surface. AADPC has more side chains substituted to aromatics, as indicated by the higher signals at 146, 129, and 80 ppm. Meanwhile, the C−O bonds, that is, those indicated by signals at 101 and 97 ppm, are restrained to break during pyrolysis. Additionally, AADPC has the highest phenolic-OH content assigned to 146 ppm. The conjugated C═O bonds, that is, those indicated by the signal at 178 ppm in AADPC, are decomposed during pyrolysis. The treated AD accelerates the cleavage of C═O bonds but suppresses C−O bond breakage to form carbon−oxygen−metal (C−O−M) structures. The carbon−alumina composite is prepared with higher carbon content in side chains on aromatics combined with metal, i.e., C−O−M structures, from AD.

Furthermore, the concentrations of Cu, Zn, Pb, and Cr in the leachate extracted, shown in Table 3, from the composite of AD and biochar were far under the threshold values required in GB5085.1-2007 and GB16889-2008. The heavy metal was immobilized in the composite.

Table 3. Heavy Metal Leaching Concentration in the Composite

sample	Cu	Zn	Pb	Cr
composite[a] (ppm)	3.20	0.21		0.020
GB5085.1 (ppm)	100	100	5	5
GB16889 (ppm)	40	100	0.25	4.5

[a]The composite is pine char catalyzed by AAD, which is called AADPC.

2.2. Effects of Operating Conditions on Cr(VI) Removal. *2.2.1. Absorbent Type.* The absorption experiments of composites prepared at different temperatures in Figure 1a show that the removal rate of Cr(VI) increases with increasing pyrolysis temperature in the range from 400 to 700 °C. In contrast, the removal efficiency by PC decreases with increasing temperature. Absorption of Cr(VI) is a complexation process influenced by the OcFGs and the minerals on the surface of sorbents. With increasing temperature, the OcFGs decompose during pyrolysis. The OcFGs in hemicellulose, such as those assigned to 15 ppm, are not detected by ^{13}C NMR in PC. The C−O bonds in amorphous cellulose, that is, those assigned to 80 ppm, disappear from PC. These OcFGs are not decomposed during pyrolysis at 700 °C and persist in ADPC. When the temperature increases to 700 °C, it has a weak $CrO_4^{2-}-\pi$ interaction combined to aromatics in PC during absorption. AD has abundant minerals that assist in enhancing Cr(VI) absorption by precipitation. The removal efficiency reaches to 77.20% (maximum value) using composite pyrolysis at 700 °C. The removal efficiency of AADPC for Cr(VI) is 88.47%, as shown in Figure 1b. It indicates that the optimum absorbent for removal of Cr(VI) is the composite from pyrolysis of pine with AD treated by organic acid. Some OcFGs remain in AADPC analyzed, as listed in Table 1. The available sites for absorbing Cr(VI) by AADPC are more than those by ADPC and PC. The adsorption capability of AADPC is greater than those of ADPC and PC, as shown in Figure 1b.

2.2.2. Adsorption Kinetics. Cr(VI) adsorption on the composite in solution follows a three-step mechanism: film diffusion, intraparticular diffusion, and adsorption equilibrium. The adsorption kinetic models that are the best fit for Cr adsorption on biochar are the pseudo-first-order and pseudo-second-order kinetic models in the previous study. These models are described in Table 4. The effect of contact time on Cr adsorption by ADPC and AADPC, as shown in Figure 2a, shows that the equilibrium time is about 60 min. The fitting curves by pseudo-first-order and pseudo-second-order kinetic models according to data in Figure 2a are shown in Figure 2b,c.

Judging from the correlation coefficient (R^2) values in Table 5, the preferable model is the pseudo-second-order kinetic model for both ADPC and AADPC (R^2 > 0.99). The assumption of the pseudo-second-order kinetic model is that the rate of Cr(VI) adsorption on the composite is proportional to the number of active sites on the composite surface, which implies that the rate-limiting step may be a chemical sorption (complex reaction with functional groups and precipitation with minerals) between Cr(VI) and the composite. The calculated value of q_e is consistent with the experimental value.

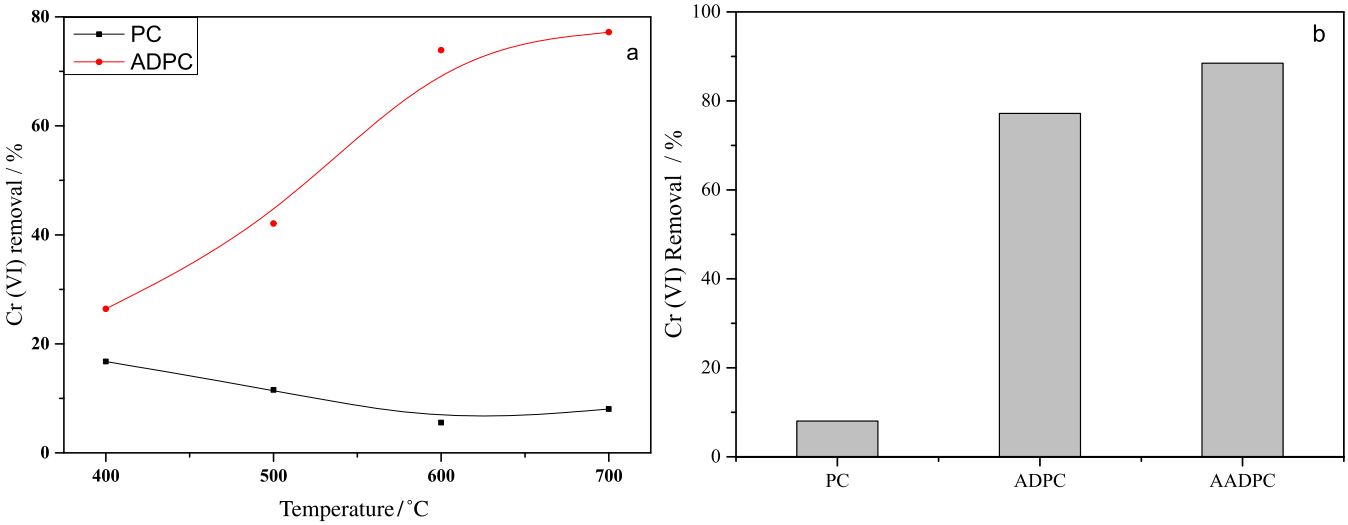

Figure 1. Effect of absorbent type on the removal efficiency for Cr(VI) with an initial concentration of 2 μg/mL: (a) comparison of PC and ADPC for Cr(VI) removal with increasing pyrolysis temperature and (b) comparison of PC, ADPC, and AADPC for Cr(VI) removal at the same condition.

https://doi.org/10.1021/acsomega.1c02998
ACS Omega 2021, 6, 22301−22310

Table 4. Adsorption Models Used in This Work and Their Parameters

model	equation	linearized form	parameters
			isotherm models
Langmuir	$q_e = \frac{q_m K_L C_e}{1 + K_L C_e}$	$\frac{C_e}{q_e} = \frac{1}{q_m K_L} + \frac{C_e}{q_m}$ $R_L = \frac{1}{1 + K_L C_0}$	q_e (μg/g): amount of metal ion adsorbed at equilibrium q_m (μg/g): complete monolayer adsorption capacity C_e (μg/L): equilibrium concentration K_L (L/μg): Langmuir adsorption constant C_0: highest initial concentration of the adsorbate in the solution (μg/L) R_L: shape of the isotherm
Freundlich	$q_e = K_F C_e^{1/n}$	$\ln q_e = \ln K_F + \frac{1}{n} \ln C_e$	n: empirical parameter related to the adsorption intensity, which varies with the heterogeneity of the material (dimensionless) K_F ($(\mu g/g)(L/\mu g)^{1/n}$): Freundlich adsorption constant
Dubinin−Radushkevich (D−R)	$q_e = q_m \exp(-\beta\varepsilon^2)$	$\ln q_e = \ln K_F - \beta\varepsilon^2$ $\varepsilon = RT \ln\left(1 + \frac{1}{C_e}\right)$	β (mol^2/kJ^2): adsorption energy constant ε: Polanyi potential
			kinetic models
pseudo-first-order	$\frac{dq_t}{dt} = k_1(q_e - q_t)$	$\ln(q_e - q_t) = \ln q_e - k_1 t$	q_e (μg/g): adsorption capacity at equilibrium q_t (μg/g): adsorption capacity at time t t (min): contact time k_1 (1/min): rate constant of pseudo-first-order adsorption
pseudo-second-order	$\frac{dq_t}{dt} = k_2(q_e - q_t)^2$	$\frac{t}{q_t} = \frac{1}{k_2 q_e^2} + \frac{t}{q_e}$	q_t (μg/g): adsorption capacity at time t k_2 (g/μg min): rate constant of pseudo-second-order adsorption

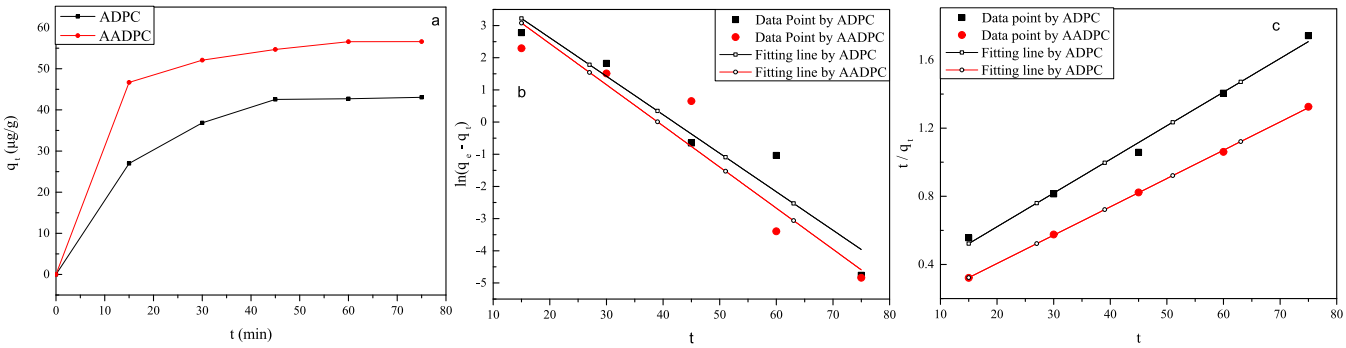

Figure 2. Effect of contact time on Cr(VI) sorption (a) and kinetic analysis by pseudo-first-order (b) and pseudo-second-order (c) models for ADPC and AADPC.

Table 5. Kinetic Parameters of Pseudo-First-Order and Pseudo-First-Order Models

	pseudo-first-order model				pseudo-second-order model		
sorbent	q_e (exp)	q_e	k_1	R^2	q_e	k_1	R^2
ADPC	43.06	150.46	0.1196	0.890	50.63	0.0017	0.991
AADPC	56.61	147.68	0.1278	0.909	60.20	0.0038	0.999

The k_1 and q_e values of the pseudo-second-order model for AADPC are greater than those for ADPC, as illustrated in Table 5. In the case of rate-limited chemisorption fitted by the pseudo-second-order model, data suggests that inner-sphere complexation and precipitation involved the metal ion sorption. Acid-treated AD (AAD) produces composites with more OcFGs and metal ions for inner-sphere complexation and precipitation. The absorption efficiency for Cr(VI) by AADPC is better than that by ADPC.

2.2.3. Adsorption Isotherms. The Cr(VI) adsorption data of ADPC and AADPC were analyzed using the Langmuir and Freundlich isotherm models, as shown in Figure 3, with the relevant isotherm parameters presented in Table 6.

Taking into account the correlation coefficient (R^2), it is the highest for the Langmuir model, indicating that the adsorption process is best described by this model. The results show that it is valid for monolayer sorption onto a surface with a finite number of identical sites on the composite. The values of the separation factor, R_L, indicating the nature of the adsorption process, are also presented in Table 6. They can be classified as follows: $R_L > 1$ unfavorable, $R_L = 1$ linear, $0 < R_L < 1$ favorable, $R_L = 0$ irreversible. The R_L of AADPC is 0.011, lower than 0.107 of ADPC. The adsorption of Cr(VI) onto AADPC is more favorable. The q_m for Cr(VI) absorption on AADPC is greater than that on ADPC. The parameters n and K_F in the Freundlich model of AADPC are also greater than those of ADPC.

2.3. Correlation of the Microstructure in the Carbon−Alumina Composite to Cr(VI) Removal. Cr(VI) adsorption is a complex mechanism influenced by the surface structure of the composite. Cr(VI) contacted the composite first to induce the "adsorption-coupled reduction" reaction through direct

https://doi.org/10.1021/acsomega.1c02998
ACS Omega 2021, 6, 22301−22310

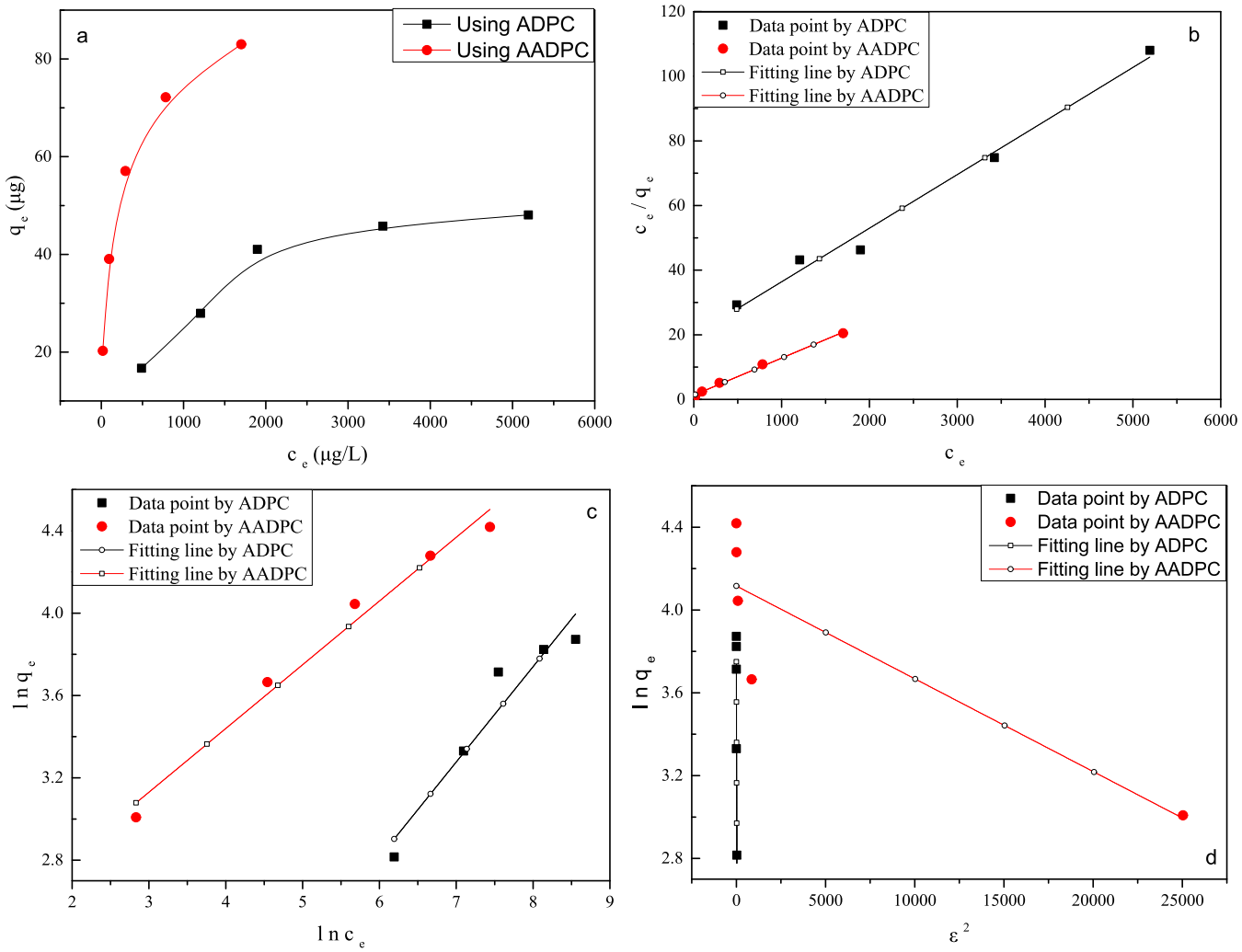

Figure 3. Adsorption isotherms of Cr(VI) onto ADPC and AADPC: (a) adsorption isotherm, (b) Langmuir isotherm model, (c) Freundlich isotherm model, and (d) Dubinin−Redushckevich (D−R) isotherm model.

Table 6. Isotherm Model Data

	Langmuir model				Freundlich model			D−R model		
sample	q_m (μg/g)	k_L (L/μg)	R_L	R^2	n	k_F (L/μg)	R^2	q_m (μg/g)	E (kJ/mol)	R^2
ADPC	60.31	0.00084	0.107	0.984	2.15	1.04	0.904	42.90	0.008	0.838
AADPC	87.26	0.00865	0.011	0.994	3.23	9.04	0.976	61.32	5.58	0.695

and indirect reduction in the solution. The direct reduction of Cr(VI) to Cr(III) proceeds in the aqueous phase by contacting with the electron-donating groups,[43−45] such as phenolic, methoxy, and carbonyl functional groups on the composite. Cr(III) ions then coprecipitate with metal cations to form complexes as the Cr-binding groups and precipitate on the surface of composites. The indirect reduction can be divided into three steps,[46,47] including (a) anionic Cr(VI) cross-links to OcFGs on the composite surface, (b) Cr(VI) reduces to Cr(III) by adjacent OcFGs, and (c) complexation or precipitation of Cr(III) on the composite surface. According to analysis of adsorption behavior, Cr(VI) adsorption fits chemisorption with monolayer sorption onto the composite surface. Chemisorption is mainly induced by complexation with OcFGs, coprecipitation with metal ions on the composite, and the cation-exchange reaction. Cr(VI) adsorption and reduction to Cr(III) through the diffusion, adsorption, complexation, reduction, and coprecipitation steps for its removal are shown in Figure 4.

Cr(VI) removal involves diffusion with absorbents from external channels to inner channels, adsorption with OcFGs in the inner channel, enhanced complexation and coprecipitation with metal ions on absorbents, and reduction to Cr(III) by absorbents.

First, compared with PC, composites, such as ADPC or AADPC, have more OcFGs analyzed by ^{13}C NMR. Cr(VI) adsorption and reduction are enhanced by complexation with OcFGs on biochar, as shown in eqs 1−3

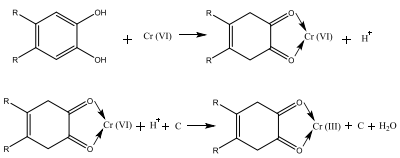

(1)

(2)

https://doi.org/10.1021/acsomega.1c02998
ACS Omega 2021, 6, 22301−22310

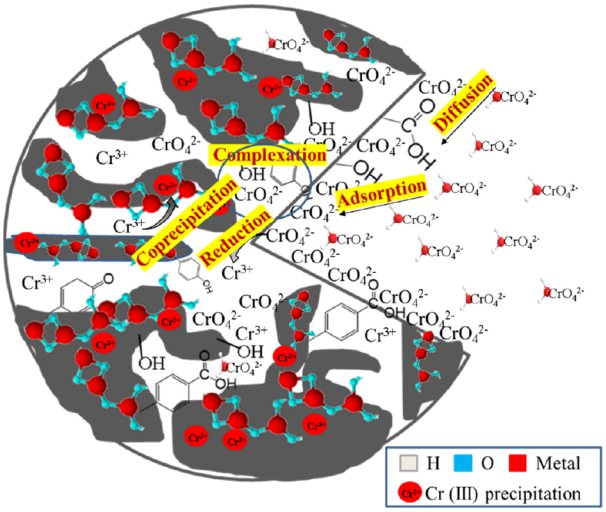

Figure 4. Mechanism on Cr(VI) removal from the aqueous solution by AADPC.

$$Cr(VI) + H^+ + Ph\text{-}OH \rightarrow Ph\text{-}O\text{-}Cr(III) + H_2O \quad (3)$$

OcFGs acting as electron donors are responsible for Cr(VI) reduction to Cr(III) and formation of complexes. The XPS spectra of Cr 2p are shown in Figure 5.

From Figure 5, it can be seen that Cr(VI) absorbed onto the composite can be reduced to Cr(III). The reduction of Cr(VI) to Cr(III) is more favorable for ADPC and AADPC than PC. The area percentage of Cr(VI) and Cr(III) based on XPS spectra of Cr 2p, shown in Figure 6a−c, of the char and composite is given in Table 7.

As discussed above in Table 1, the metallic oxide in AD combines with biomass components and organic products by van der Waals forces and hydrogen bonds to form C−O−M intermediates during copyrolysis. The C−O−M intermediates assist the complex formation during absorption. OcFGs, such as the alcohol hydroxyl group substituted to glucosyl units in amorphous cellulose and hemicellulose, assigned to 70−110 ppm, and the phenolic group in lignin, assigned to 120−150 ppm, remain in the ADPC composite. These functional groups have significant influence on the "adsorption-coupled reduction" reaction of Cr(VI) removal from a solution. The reaction pathway is illustrated by eqs 3−7

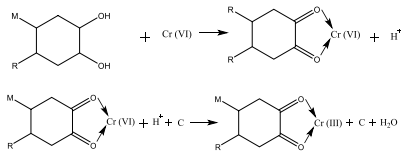

(4)

(5)

The carbonyl group in hemicellulose assigned to 15 ppm also contributes to absorption of Cr(VI) induced by eqs 6 and 7

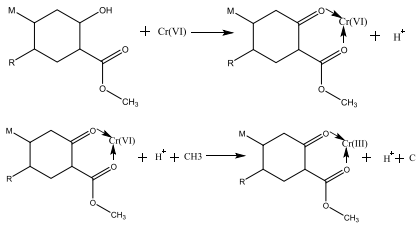

(6)

(7)

The above results show clearly the preferable Cr(VI) adsorption of ADPC in comparison to PC. As for AADPC, the copyrolysis product from pine and AAD has also more alcohol hydroxyl groups substituted to glucosyl units in amorphous cellulose and hemicellulose, assigned respectively to 80, and 97 and 101 ppm, as illustrated in Table 2. Also, it has more phenolic groups in lignin distributed at syringyl units assigned to 129 and 146 ppm. These organic carbon structures aid to the excellent Cr(VI) removal of 95.08% at 60 °C for 60 min with an initial concentration of 6 mg/L. In total, 41.08% of Cr(VI) from the solution is reduced to Cr(III), as shown in Table 7.

Second, the main composition in AD is Al_2O_3. Al_2O_3 is used as a water purifying agent for its flocculating property in the solution; it reacts with water to form $Al(OH)_3$, as shown in eq 8

$$Al_2O_3 + H_2O \rightarrow Al(OH)_3 + H^+ \quad (8)$$

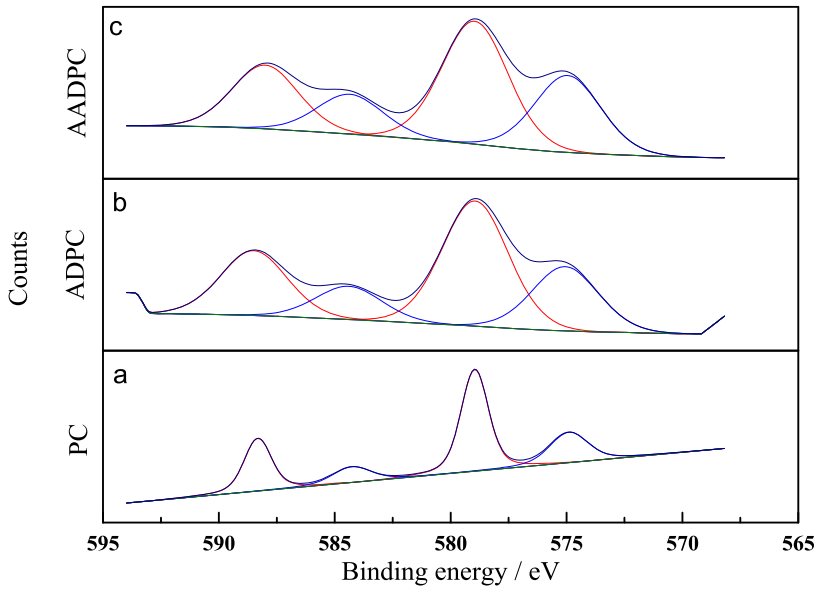

Figure 5. Valence state variation of Cr 2p on the surface of the char and composite: (a) PC, (b) ADPC, and (c) AADPC.

https://doi.org/10.1021/acsomega.1c02998
ACS Omega 2021, 6, 22301−22310

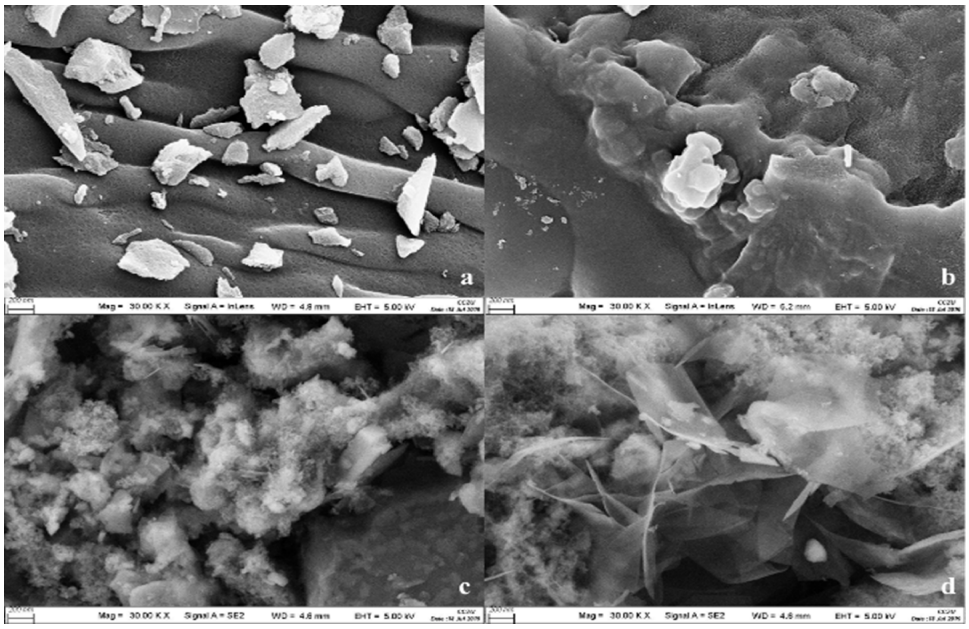

Figure 6. SEM images of PC and AADPC before and after adsorption: (a) PC before adsorption, (b) PC after adsorption, (c) AADPC before adsorption, and (d) AADPC after adsorption.

Table 7. Area Percentage of Fitting Curves from XPS Spectra of Cr 2p on the Surface of Char

sample	PC	ADPC	AADPC
Cr(VI)	70.53	66.13	58.92
Cr(III)	29.47	33.87	41.08

The composite of AADPC not only has abundant OcFGs to provide active sites for Cr(VI) removal on char surface but also has metal cations for coprecipitation. AADPC has higher hydrophilicity and reducing potential with more OcFGs. Hydrated chromium ions diffuse into micro- or ultra-micropores in the composite and combine with OcFGs. Chromium ions can adsorb on these micropores and composite surface. However, according to data in Table 1, the OcFGs in PC are fewer; there are almost pure, solid, hydrophobic carbons on the pore wall surfaces, so water cannot diffuse into that solid. Compared with the scanning electron microscopy (SEM) images of PC and AADPC shown in Figure 6, AADPC has more floccular lamella on the composite surface after adsorption, evidencing the coprecipitation of metal cations with chromium ions.

The C−O−M structures are more favorable for forming complexes with Cr(VI) by flocculation and coprecipitation. Furthermore, the PC surface is smooth and AADPC is rough with many floccular pellets, as shown in Figure 6. The pellets provide more active sites on the surface for Cr(VI) adsorption.

In short, the "adsorption-coupled reduction" reaction for Cr(VI) removal from the solution, including diffusion, adsorption, complexation, reduction, and coprecipitation, is influenced by OcFGs and metal ions on the surface of AADPC. The number of active sites on AADPC is greater than those on ADPC and PC with higher OcFGs.

3. CONCLUSIONS

OcFGs in the composite have a significant influence on Cr(VI) removal and stabilization with the "adsorption-coupled reduction" reaction. AADPC with higher OcFGs is prepared by copyrolysis of pine and AD pretreated with organic acid. The organic acid is the byproduct from biomass pyrolysis and reused for activation of AD. Based on the results discussed, the conclusions are as follows:

(1) AD addition selectively sustains C−O bonds to prepare the C−O−M composite with higher OcFGs. AADPC has more alcohol hydroxyl groups substituted to glucosyl units assigned to 80 ppm (12.71%) in amorphous cellulose and 97 ppm (6.47%) and 101 ppm (7.66%) in hemicellulose. Also, it has more phenolic groups in lignin distributed at syringyl units assigned to 129 and 146 ppm, with a total content of 24.35%. These organic carbon contents are all higher than those in PC and ADPC.

(2) AADPC is an excellent sorbent for Cr(VI) removal and stabilization. The Cr(VI) adsorption process is described with the Langmuir thermodynamic model and the pseudo-second-order kinetic model. The optimal removal is 95.08% at 60 °C for 60 min with an initial Cr(VI) concentration of 6 mg/L.

(3) AADPC synergizes the functions of biochar and metallic oxide to induce a series of processes, including diffusion, adsorption, complexation, reduction, and coprecipitation, for Cr(VI) removal and immobilization.

These results provide a new direction for the reuse of organic and industrial solid wastes to realize the goal of comprehensive utilization of various waste materials for high-performance adsorption material production.

4. MATERIALS AND METHODS

4.1. Materials. Pine sawdust collected from south of Anhui Province in China was used as the raw material and ground to <0.2 mm. AD was produced from the dross recycling process in secondary smelters in Changzhou smashed to <0.2 mm. The main chemical composition of AD as analyzed by an X-ray fluorescence (XRF) spectrometer (S8 Tiger, Bruker AXS, Germany) is shown in Table 1.

https://doi.org/10.1021/acsomega.1c02998
ACS Omega 2021, 6, 22301−22310

Table 8. Chemical Composition of AD and AAD

compound	Al_2O_3	SiO_2	Na_2O	MgO	CuO	Fe_2O_3	K_2O	CaO	ZnO
AD	80.38	6.12	4.46	4.53	0.68	0.83	0.54	0.39	0.20
AAD	78.61	7.61	4.55	4.18	0.89	0.99	0.66	0.51	0.23

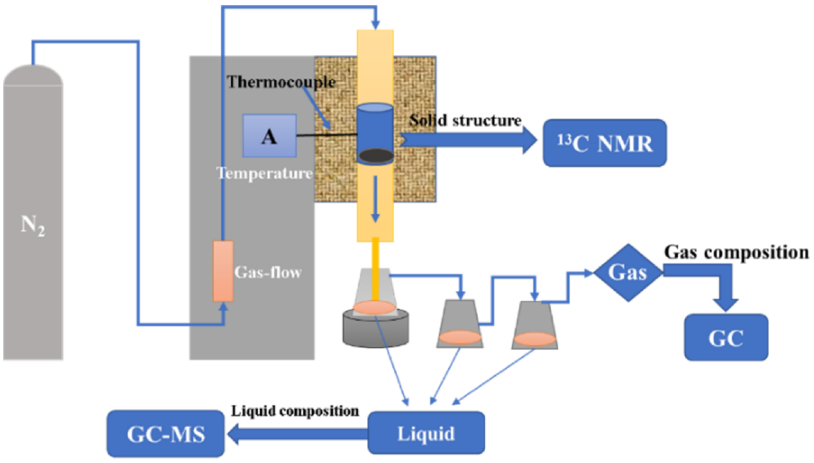

Figure 7. Schematic diagram of the pyrolysis experiment.

4.2. AD Pretreated with the Liquid Product from Pine Pyrolysis (AAD). AD (20 g) was uniformly mixed with 20 mL of liquid product, whose main composition was organic acids from pine pyrolysis, and then calcined in a muffle furnace at 550 °C for 2 h. AAD was prepared, and the chemical composition of AD and AAD as analyzed by XRF spectrometer is presented in Table 8.

4.3. Pyrolysis. AD or AAD was mixed with pine sawdust by mass ratio using mechanical stirring. Pyrolysis tests were carried out in a vertical quartz tubular reactor. The gas−liquid separator was connected with the reactor through ground glass. Pure pine sawdust or a 1:1 mixture of pine sawdust and AD (or AAD) was placed in the reactor. N_2 was led into the reactor at 90 mL/min as a carrier gas. The reactor was heated to the set temperature at a heating rate of 10 °C /min. The char from pine pyrolysis was denoted PC, the composite from copyrolysis of AD and pine was denoted ADPC, and the composite from copyrolysis of AAD and pine was denoted AADPC. The schematic diagram of the pyrolysis experiment is shown in Figure 7.

4.4. Cr(VI) Analysis and Adsorption Experiments. *4.4.1. Cr(VI) Analysis.* In this experiment, 2 μg/mL standard stock solutions of Cr(VI) were prepared by dissolving specific amounts of K_2CrO_4 in pure water. In a set of 100 mL volumetric flasks, 0, 1.00, 2.00, 4.00, 7.00, and 10.00 mL of standard stock solution of Cr(VI) were added. Sulfuric acid solution (1 mL) was then added, followed by predilution with water to about 90 mL; 3 mL of diphenyl carbazide ethanol solution was then added and finally diluted to 100 mL with water under vigorous shaking and mixing. The absorbance was measured using a UV spectrophotometer at a wavelength of 540 nm. The working curve was drawn by taking the chromium content as the abscissa and the corresponding absorbance as the ordinate. The concentration of Cr(VI) was calculated by the working curve.

4.4.2. Adsorption Experiments. Adsorption experiments were carried out in a series of beakers containing 10 mL of Cr(VI) (2, 4, 6, 8, and 10 μg/mL) using PC, ADPC, and AADPC samples (1.0000 g). The experiments were performed on a magnetic stirrer under the experimental conditions of 100 rpm and 60 °C to a state of equilibrium (about 60 min). Therein, 6 μg/mL Cr(VI) solution was used to analyze the effect of adsorption time (15, 30, 45, 60, and 75 min) on the amount of adsorbate for the adsorption kinetic study. The absorbance of the solution was measured using a UV spectrophotometer and calculated by working curves after filtration using a 0.45 μm membrane. The removal efficiency was calculated by eq 9

$$\text{removal efficiency (\%)} = \frac{(C_0 - C_e)}{C_0} \times 100 \tag{9}$$

The amount of the adsorbate removed by the adsorbent, q (μg/g), was calculated using eq 10

$$q_e = \frac{(C_0 - C_e)}{m \times V} \tag{10}$$

where C_0 (μg/L) and C_e (μg/L) represent the initial and equilibrium concentrations of Cr(VI), respectively, V (L) is the volume of the solution, and m (g) is the mass of the adsorbent.

4.5. Analytical Methods. *4.5.1. Characterization of Carbon Structures and Surface Properties of Solid Products.* The organic carbon structures of pine, PC, ADPC, and AADPC were investigated by ^{13}C NMR. ^{13}C MAS NMR experiments of biomass were performed on an Agilent 600 DD2 spectrometer at a resonance frequency of 150.15 MHz, as described in our previous work.[48] The surface microstructures of PC and AADPC were characterized by SEM. The BET surface areas and the total pore volumes of AD and AAD were calculated based on the N_2 adsorption−desorption isotherms measured by a gas sorption analyzer (ASAP2460, USA).

4.5.2. Leaching Behavior of Heavy Metals in Solid Products from Pyrolysis. Samples were first analyzed to obtain general element species and contents by XRF spectroscopy. Then, the leaching tests were performed according to the "Chinese Standard Solid Waste Extraction Procedure for Leaching Toxicity-Acetic Acid Buffer Solution Method" (HJ/T300-2007); after the preliminary evaluation of

https://doi.org/10.1021/acsomega.1c02998
ACS Omega 2021, 6, 22301−22310

the pH characteristic of the sample, CH_3COOH solution (pH = 2.64 ± 0.05) was chosen as the exaction fluid for the experiment. This fluid was prepared by adding 17.25 mL of glacial acetic acid into 1 L of deionized water. Then, 1 g of sample was placed in a 50 mL centrifugal tube, and 20 mL of extraction fluid was added to each tube (including the control sample). The samples were then agitated for 18 h with an electric stirrer. The suspension was filtered through a polypropylene filter (0.45 μm) and acidified with concentrated nitric acid to decrease the pH of the obtained water sample between 1 and 2 and then were analyzed using an atomic absorption spectrophotometer (AAS300, Analytik Jena, Germany). The leaching method was similar to the toxicity characteristic leaching procedure.

■ ASSOCIATED CONTENT

Supporting Information

The Supporting Information is available free of charge at https://pubs.acs.org/doi/10.1021/acsomega.1c02998.

Fitted ^{13}C NMR spectra (Figure S1), carbon structure assigned to the chemical shift (Table S1), and carbon structure units of biomass (Figure S2) (PDF)

■ AUTHOR INFORMATION

Corresponding Authors

Zhengzhong Zhou − *National-Local Joint Engineering Research Center of Biomass Refining and High-Quality Utilization, Institute of Urban and Rural Mining, Changzhou University, Changzhou, Jiangsu 213164, China*; Email: zhouzhengzhong@cczu.edu.cn

Tingzhou Lei − *National-Local Joint Engineering Research Center of Biomass Refining and High-Quality Utilization, Institute of Urban and Rural Mining, Changzhou University, Changzhou, Jiangsu 213164, China*; Email: china_newenergy@163.com

Authors

Peng Liu − *Jiangsu Province Biomass Energy and Materials Laboratory, Nanjing 210042, China; National-Local Joint Engineering Research Center of Biomass Refining and High-Quality Utilization, Institute of Urban and Rural Mining, Changzhou University, Changzhou, Jiangsu 213164, China*; orcid.org/0000-0003-2418-5030

Li Liu − *National-Local Joint Engineering Research Center of Biomass Refining and High-Quality Utilization, Institute of Urban and Rural Mining, Changzhou University, Changzhou, Jiangsu 213164, China*

Yanling Li − *National-Local Joint Engineering Research Center of Biomass Refining and High-Quality Utilization, Institute of Urban and Rural Mining, Changzhou University, Changzhou, Jiangsu 213164, China*

Taoli Huhe − *National-Local Joint Engineering Research Center of Biomass Refining and High-Quality Utilization, Institute of Urban and Rural Mining, Changzhou University, Changzhou, Jiangsu 213164, China*

Complete contact information is available at: https://pubs.acs.org/10.1021/acsomega.1c02998

Notes

The authors declare no competing financial interest.

■ ACKNOWLEDGMENTS

This study was funded by the Foundation from Jiangsu Province Biomass Energy and Materials Laboratory (no. JSBEM202004), the Natural Science Foundation of China (no. 51906021), the High Quality Energy Development Strategy Research in Shandong Province (no. 201901SDZD01), and Energy Revolution Strategy Research of Henan Province.

■ REFERENCES

(1) Cai, Y.; Feng, J.; Tan, X.; Wang, X.; Lv, Z.; Chen, W.; Fang, M.; Liu, H.; Wang, X. Efficient capture of $ReO4^-$ on magnetic amine-functionalized MIL-101 (Cr): Revealing from selectivity to mechanism. *Sci. Total Environ.* **2021**, *771*, No. 144840.

(2) Chen, Z.; Wei, D.; Li, Q.; Wang, X.; Yu, S.; Liu, L.; Liu, B.; Xie, S.; Wang, J.; Chen, D.; Hayat, T.; Wang, X. Macroscopic andcroscopic investigation of Cr(VI) immobilization by nanoscaled zero-valent iron supported zeolite MCM-41 vis batch, visual, XPS and EXAFS techniques. *J. Cleaner Prod.* **2018**, *181*, 745−752.

(3) Liu, Y.; Huo, Y.; Wang, X.; Yu, S.; Ai, Y.; Chen, Z.; Zhang, P.; Chen, L.; Song, G.; Alharbi, N. S.; Rabah, S. O.; Wang, X. Impact of metal ions and organic ligands on uranium removal properties by zeolitic imidazolate framework materials. *J. Cleaner Prod.* **2021**, *278*, No. 123216.

(4) Wang, Z. Y.; Wang, Y. C.; Wang, W. J.; Tao, S. N.; Chen, Y. F.; Tang, M.; Shao, D. D.; Xing, W.; Sun, S. P. Designing scalable dual-layer composite hollow fiber nanofiltration membranes with fully cross-linked ultrathin functional layer. *J. Membr. Sci.* **2021**, *628*, No. 119243.

(5) Gossuin, Y.; Vuong, Q. L. NMR relaxometry for adsorption studies: Proof of concept with copper adsorption on activated alumina. *Sep. Purif. Technol.* **2018**, *202*, 138−143.

(6) Haddad, A. Z.; Pilgrim, C. D.; Sawvel, A. M.; Hohman, J. N.; Gadgil, A. J. On the Conversion of Bauxite Ores to Highly Activated Alumina Media for Water Remediation. *Adv. Sustainable Syst.* **2019**, *3*, No. 1900005.

(7) Mahinroost, M.; Allahverdi, A. Hazardous aluminum dross characterization and recycling strategies: A critical review. *J. Environ. Manage.* **2018**, *223*, 452−468.

(8) Gil, A.; Arrieta, E.; Vicente, M. A.; Korili, S. A. Application of Industrial Wastes from Chemically Treated Aluminum Saline Slags as Adsorbents. *ACS Omega* **2018**, *3*, 18275−18284.

(9) Adeosun, S. O.; Sekunowo, O. I.; Taiwo, O. O.; Ayoola, W. A.; Machado, A. Physical and mechanical properties of aluminum dross. *Adv. Mater.* **2014**, *3*, 6−10.

(10) David, E.; Kopac, J. The Assessment of the Recycling Process of Aluminum Hazardous Waste and a New Route of Development. *Mater. Today: Proc.* **2019**, *10*, 340−347.

(11) Vavva, C.; Voutsas, E.; Magoulas, K. Process development for chemical stabilization of fly ash from municipal solid waste incineration. *Chem. Eng. Res. Des.* **2017**, *125*, 57−71.

(12) Zeng, J.; Yue, Y.; Gao, Q.; Zhang, J.; Zhou, J.; Pan, Y.; Qian, G.; Tang, J.; Ruan, J. Co-treatment of hazardous wastes by the thermal plasma to produce an effective catalyst. *J. Cleaner Prod.* **2019**, *208*, 243−251.

(13) Berezin, B. B.; Bezrodnykh, E. A.; Blagodatskikh, I. V.; Yamskov, I. A.; Tikhonov, V. E. Extraction of residual heavy metals from commercial chitosan and approach to preparation of oligochitosan hydrochloride. *Carbohydr. Polym.* **2019**, *215*, 316−321.

(14) Dou, X.; Chen, D.; Hu, Y.; Feng, Y.; Dai, X. Carbonization of heavy metal impregnated sewage sludge oriented towards potential co-disposal. *J. Hazard. Mater.* **2017**, *321*, 132−145.

(15) Hadi, P.; Xu, M.; Ning, C.; Ki Lin, C. S.; McKay, G. A critical review on preparation, characterization and utilization of sludge-derived activated carbons for wastewater treatment. *Chem. Eng. J.* **2015**, *260*, 895−906.

(16) Chen, F.; Hu, Y.; Dou, X.; Chen, D.; Dai, X. Chemical forms of heavy metals in pyrolytic char of heavy metal-implanted sewage sludge

and their impacts on leaching behaviors. *J. Anal. Appl. Pyrolysis* **2015**, *116*, 152−160.
(17) Liu, T.; Liu, Z.; Zheng, Q.; Lang, Q.; Xia, Y.; Peng, N.; Gai, C. Effect of hydrothermal carbonization on migration and environmental risk of heavy metals in sewage sludge during pyrolysis. *Bioresour. Technol.* **2018**, *247*, 282−290.
(18) Leng, L.; Leng, S.; Chen, J.; Yuan, X.; Li, J.; Li, K.; Wang, Y.; Zhou, W. The migration and transformation behavior of heavy metals during co-liquefaction of municipal sewage sludge and lignocellulosic biomass. *Bioresour. Technol.* **2018**, *259*, 156−163.
(19) Huber, F.; Blasenbauer, D.; Mallow, O.; Lederer, J.; Winter, F.; Fellner, J. Thermal co-treatment of combustible hazardous waste and waste incineration fly ash in a rotary kiln. *Waste Manage.* **2016**, *58*, 181−190.
(20) Yao, Y.; Gao, B.; Zhang, M.; Inyang, M.; Zimmerman, A. R. Effect of biochar amendment on sorption and leaching of nitrate, ammonium, and phosphate in a sandy soil. *Chemosphere* **2012**, *89*, 1467−1471.
(21) Shen, Z.; Zhang, Y.; McMillan, O.; Jin, F.; Al-Tabbaa, A. Characteristics and mechanisms of nickel adsorption on biochars produced from wheat straw pellets and rice husk. *Environ. Sci. Pollut. Res.* **2017**, *24*, 12809−12819.
(22) Vithanage, M.; Mayakaduwa, S. S.; Herath, I.; Ok, Y. S.; Mohan, D. Kinetics, thermodynamics and mechanistic studies of carbofuran removal using biochars from tea waste and rice husks. *Chemosphere* **2016**, *150*, 781−789.
(23) Herath, I.; Kumarathilaka, P.; Al-Wabel, M. I.; Abduljabbar, A.; Ahmad, M.; Usman, A. R. A.; Vithanage, M. Mechanistic modeling of glyphosate interaction with rice husk derived engineered biochar. *Microporous Mesoporous Mater.* **2016**, *225*, 280−288.
(24) Mayakaduwa, S. S.; Kumarathilaka, P.; Herath, I.; Ahmad, M.; Al-Wabel, M.; Ok, Y. S.; Usman, A.; Abduljabbar, A.; Vithanage, M. Equilibrium and kinetic mechanisms of woody biochar on aqueous glyphosate removal. *Chemosphere* **2016**, *144*, 2516−2521.
(25) Wathukarage, A.; Herath, I.; Iqbal, M. C. M.; Vithanage, M. Mechanistic understanding of crystal violet dye sorption by woody biochar: Implications for wastewater treatment. *Environ. Geochem. Health* **2019**, *41*, 1647−1661.
(26) Ahmad, M.; Rajapaksha, A. U.; Lim, J. E.; Zhang, M.; Bolan, N.; Mohan, D.; Vithanage, M.; Lee, S. S.; Ok, Y. S. Biochar as a sorbent for contaminant management in soil and water: A review. *Chemosphere* **2014**, *99*, 19−33.
(27) Agrafioti, E.; Kalderis, D.; Diamadopoulos, E. Arsenic and chromium removal from water using biochars derived from rice husk, organic solid wastes and sewage sludge. *J. Environ. Manage.* **2014**, *133*, 309−314.
(28) Zhang, W.; Mao, S.; Chen, H.; Huang, L.; Qiu, R. Pb(II) and Cr(VI) sorption by biochars pyrolyzed from the municipal wastewater sludge under different heating conditions. *Bioresour. Technol.* **2013**, *147*, 545−552.
(29) Zhou, F.; Wang, H.; Fang, S.; Zhang, W.; Qiu, R. Pb(II), Cr(VI) and atrazine sorption behavior on sludge-derived biochar: Role of humic acids. *Environ. Sci. Pollut. Res.* **2015**, *22*, 16031−16039.
(30) Xue, Y.; Wang, C.; Hu, Z.; Zhou, Y.; Xiao, Y.; Wang, T. Pyrolysis of sewage sludge by electromagnetic induction: Biochar properties and application in adsorption removal of Pb(II), Cd(II) from aqueous solution. *Waste Manage.* **2019**, *89*, 48−56.
(31) Premarathna, K. S. D.; Rajapaksha, A. U.; Sarkar, B.; Kwon, E. E.; Bhatnagar, A.; Ok, Y. S.; Vithanage, M. Biochar-based engineered composites for sorptive decontamination of water: A review. *Chem. Eng. J.* **2019**, *372*, 536−550.
(32) Zhang, P.; O'Connor, D.; Wang, Y.; Jiang, L.; Xia, T.; Wang, L.; Tsang, D. L. C. W.; Ok, Y. S.; Hou, D. A green biochar/iron oxide composite for methylene blue removal. *J. Hazard. Mater.* **2020**, *384*, No. 121286.
(33) Frišták, V.; Micháleková-Richveisová, B.; Víglašová, E.; Ďuriška, L.; Galamboš, M.; Moreno-Jimenéz, E.; Pipíška, M.; Soja, G. Sorption separation of Eu and As from single-component systems by Fe-modifed biochar: Kinetic and equilibrium study. *J. Iran. Chem. Soc.* **2017**, *14*, 521−530.
(34) Agrafioti, E.; Kalderis, D.; Diamadopoulos, E. Ca and Fe modified biochars as adsorbents of arsenic and chromium in aqueous solutions. *J. Environ. Manage.* **2014**, *146*, 444−450.
(35) Zhang, M.; Gao, B.; Yao, Y.; Xue, Y.; Inyang, M. Synthesis of porous MgO-biochar nanocomposites for removal of phosphate and nitrate from aqueous solutions. *Chem. Eng. J.* **2012**, *210*, 26−32.
(36) Wang, M. C.; Sheng, G. D.; Qiu, Y. P. A novel manganese-oxide/biochar composite for efficient removal of lead(II) from aqueous solutions. *Int. J. Environ. Sci. Technol.* **2015**, *12*, 1719−1726.
(37) Li, Y.; Wang, Z.; Xie, X.; Zhu, J.; Li, R.; Qin, T. Removal of Norfloxacin from aqueous solution by clay-biochar composite prepared from potato stem and natural attapulgite. *Colloids Surf., A* **2017**, *514*, 126−136.
(38) Wang, S.; Gao, B.; Zimmerman, A. R.; Li, Y.; Ma, L.; Harris, W. G.; Migliaccio, K. W. Removal of arsenic by magnetic biochar prepared from pinewood and natural hematite. *Bioresour. Technol.* **2015**, *175*, 391−395.
(39) Yao, Y.; Gao, B.; Fang, J.; Zhang, M.; Chen, H.; Zhou, Y.; Creamer, A. E.; Sun, Y.; Yang, L. Characterization and environmental applications of clay−biochar composites. *Chem. Eng. J.* **2014**, *242*, 136−143.
(40) Chen, L.; Chen, X. L.; Zhou, C. H.; Yang, H. M.; Ji, S. F.; Tong, D. S.; Zhong, Z. K.; Yu, W. H.; Chu, M. Q. Environmental-friendly montmorillonite-biochar composites: Facile production and tunable adsorption-release of ammonium and phosphate. *J. Cleaner Prod.* **2017**, *156*, 648−659.
(41) Karmacharya, M. S.; Gupta, V. K.; Tyagia, I.; Agarwal, S.; Jha, V. K. Removal of As(III) and As(V) using rubber tire derived activated carbon modified with alumina composite. *J. Mol. Liq.* **2016**, *216*, 836−844.
(42) Wu, P.; Cui, P.; Alves, M. E.; Peijnenburg, W. J. G. M.; Liu, C.; Zhou, D.; Wang, H.; Ok, Y. S.; Wang, Y. Interactive effects of rice straw biochar and γ-Al_2O_3 on immobilization of Zn. *J. Hazard. Mater.* **2019**, *373*, 250−257.
(43) Choppala, G.; Bolan, N.; Kunhikrishnan, A.; Bush, R. Differential effect of biochar upon reduction-induced mobility and bioavailability of arsenate and chromate. *Chemosphere* **2016**, *144*, 374−381.
(44) Wang, H. H.; Guo, H.; Zhang, N.; Chen, Z. S.; Hu, B. W.; Wang, X. K. Enhanced Photoreduction of U(VI) on C 3 N 4 by Cr(VI) and Bisphenol A: ESR, XPS, and EXAFS Investigation. *Environ. Sci. Technol.* **2019**, *53*, 6454−6461.
(45) Zhu, Y. L.; He, X. Y.; Xu, J. L.; Fu, Z.; Wu, S. Y.; Ni, J.; Hu, B. W. Insight into efficient removal of Cr(VI) by magnetite immobilized with Lysinibacillus sp. JLT12: Mechanism and performance. *Chemosphere* **2021**, *262*, No. 127901.
(46) Saha, B.; Orvig, C. Biosorbents for hexavalent chromium elimination from industrial and municipal effluents. *Coord. Chem. Rev.* **2010**, *254*, 2959−2972.
(47) Li, X.; Wang, C.; Zhang, J.; Liu, J.; Liu, B.; Chen, G. Preparation and application of magnetic biochar in water treatment: A critical review. *Sci. Total Environ.* **2020**, *711*, No. 134847.
(48) Liu, P.; Wang, Y.; Zhou, Z.; Yuan, H.; Zheng, T.; Chen, Y. Effect of carbon structure on hydrogen release derived from different biomass pyrolysis. *Fuel* **2020**, *271*, No. 117638.

https://doi.org/10.1021/acsomega.1c02998
ACS Omega 2021, 6, 22301−22310